

## Screening effects in the electron bremsstrahlung from heavy ions

M. E. Groshev <sup>1</sup>, V. A. Zaytsev,<sup>1</sup> V. A. Yerokhin,<sup>2</sup> P.-M. Hillenbrand <sup>3,4</sup>, Yu. A. Litvinov <sup>3</sup>, and V. M. Shabaev <sup>1</sup>

<sup>1</sup>*Department of Physics, St. Petersburg State University, Universitetskaya Naberezhnaya 7/9, 199034 St. Petersburg, Russia*

<sup>2</sup>*Center for Advanced Studies, Peter the Great St. Petersburg Polytechnic University, St. Petersburg 195251, Russia*

<sup>3</sup>*GSI Helmholtzzentrum für Schwerionenforschung, 64291 Darmstadt, Germany*

<sup>4</sup>*Institut für Kernphysik, Goethe-Universität, 60438 Frankfurt, Germany*



(Received 8 December 2021; revised 12 April 2022; accepted 19 April 2022; published 4 May 2022)

A fully relativistic approach is presented for the calculation of the bremsstrahlung emitted by an electron scattered off an ionic target. The ionic target is described as a combination of a nuclear electrostatic potential and a screening potential induced by the electronic cloud of the ion. The approach allows us to investigate the influence of the target electrons on the properties of the emitted radiation. We calculate the double differential cross section and Stokes parameters of the bremsstrahlung of an electron scattered off uranium ions in different charge states, ranging from bare to neutral uranium. Results on the high-energy endpoint of the electron bremsstrahlung from Li-like uranium ions  $U^{89+}$  are compared to the recent experimental data. For this process, it is found that taking into account the screening effect leads to a change of the cross section on the level of 14%, which can, in principle, be seen in present-day experiments.

DOI: [10.1103/PhysRevA.105.052803](https://doi.org/10.1103/PhysRevA.105.052803)

### I. INTRODUCTION

Electron bremsstrahlung is a process of the photon emission induced by the electron deceleration in the field of the ionic or atomic target. Investigations of this process are both of fundamental and of practical interest since they can provide information about the electronic structure and polarization properties of the target (see, e.g., reviews [1,2]).

Experimentally, bremsstrahlung is most studied for neutral atomic targets. The state-of-the-art theoretical calculations rely on the partial-wave representation of the Dirac electron wave function in the field of a finite-range central potential. This approach provides results in a remarkable agreement with experiment [3–9]. For incident electrons with energies above a few hundred keV, the dominant contribution to the bremsstrahlung comes from the scattering off the nuclear field, whereas the contribution of the electronic cloud is small. In this case, the field of the atomic target is often replaced with the pure Coulomb potential [10–13]. At higher collision energies starting from several MeV and large momentum transfers (corresponding to large photon emission angles), the extended size of the nucleus becomes significant and needs to be taken into account. The corresponding theoretical calculations are performed with the Dirac wave functions in the electrostatic potential of the nuclear charge distribution [2,14].

Recently it became possible to study the bremsstrahlung in collisions of electrons with highly charged ions [15–17]. Since it is difficult to form a target made of highly charged ions, the actual study is performed in the inverse kinematics. Namely, a beam of highly charged ions collides with a cloud of light neutral atoms. During the collision, the quasifree electron of the target is ionized and captured into the continuum of the heavy-ion projectile with simultaneous emission of a photon.

This process is called the radiative electron capture to the continuum (RECC). In the projectile rest frame, the RECC process is approximately equivalent to the bremsstrahlung in which the emitted radiation takes away the entire energy of the incoming electron, the so-called high-energy endpoint of the bremsstrahlung spectrum.

So far, theoretical studies of the RECC process (see calculations in Refs. [15–17]) were carried out under the assumption that the field of the heavy ion is represented by the pure Coulomb potential. In such an approach, the influence of the ion's electronic cloud on the properties of the emitted radiation is neglected. However, for collision energies around tens of keV used in actual experiments [15–17], the electrons of the projectile may yield a sizable effect on the properties of the emitted radiation. Here we work out a formalism for calculating the bremsstrahlung from an electron scattered off a combination of the Coulomb potential and a finite-range potential induced by the electron cloud of the ion.

Our formalism can be viewed as an extension of one developed by Yerokhin and Surzhykov [5] where the cases of the pure Coulomb and a finite-range potential were implemented. The particular form of the potential is important since it defines the asymptotic behavior of the Dirac wave function at long radial distances. In order to perform radial integrations with highly oscillating functions, we use the method of the complex-plane rotation of the integration contour, which relies on the analytical properties of the Dirac wave functions in the asymptotic region. The Dirac solutions for a finite-range potential at long distances are represented by spherical Bessel functions, which is the simplest case for the complex-plane rotation. For the pure Coulomb potential, the Dirac wave functions are described by the regular at the origin solution of the Dirac-Coulomb equation, i.e., the Whittaker function

of the first kind  $M_{\alpha\beta}$ . For the sum of the Coulomb and a finite-range potential, the Dirac wave functions at long distances are represented by a linear superposition of the regular and irregular Dirac-Coulomb wave functions. This significantly complicates the numerical implementation of the complex-plane rotation method of computation of radial integrals.

In the present paper, we apply the developed method for calculating the bremsstrahlung emitted by electrons scattered off uranium ions. By comparing the results obtained for different charge states of the ion, we study the screening effects of the target electrons on the angular distribution and polarization of the emitted photons. We also calculate the triple differential cross section of RECC for Li-like uranium studied experimentally in Ref. [17]. The theoretical results are found to be in good agreement with the experimental data. It is found that the presence of the projectile electrons modify the cross section of this process by 14%. This is comparable with the experimental uncertainty of Ref. [17] but can be detected in dedicated future experiments.

The paper is organized as follows. In Sec. II we recall basic relations for the electron bremsstrahlung. The double differential cross section and the Stokes parameters are discussed in Secs. III A and III B, respectively. Section III C is devoted to the comparison of the obtained results with the experimental data from Ref. [17]. Finally, a summary is given in Sec. IV.

Relativistic units ( $m_e = \hbar = c = 1$ ) and the Heaviside charge units ( $e^2 = 4\pi\alpha$ ) are utilized throughout the paper.

## II. BASIC FORMALISM

A fully differential cross section of the electron bremsstrahlung in the field of the ionic or atomic target is given by

$$\frac{d\sigma_{\mathbf{p}_f\mu_f,\mathbf{k}\lambda;\mathbf{p}_i\mu_i}}{d\omega d\Omega_k d\Omega_{p_f}} = (2\pi)^4 \omega^2 \frac{p_f \varepsilon_f \varepsilon_i}{p_i} |\tau_{\mathbf{p}_f\mu_f,\mathbf{k}\lambda;\mathbf{p}_i\mu_i}|^2, \quad (1)$$

where  $\varepsilon$ ,  $\mathbf{p}$ , and  $\mu$  are the energy, asymptotic momentum, and polarization of the electron in the initial ( $i$ ) and final ( $f$ ) states,  $p = |\mathbf{p}|$ ,  $(\omega, \mathbf{k})$  is the four-momentum of the emitted photon with the polarization  $\lambda$ . The amplitude is expressed by

$$\tau_{\mathbf{p}_f\mu_f,\mathbf{k}\lambda;\mathbf{p}_i\mu_i} = \int d^3\mathbf{r} \Psi_{\mathbf{p}_f\mu_f}^{(-)\dagger}(\mathbf{r}) \hat{R}_{\mathbf{k}\lambda}^\dagger(\mathbf{r}) \Psi_{\mathbf{p}_i\mu_i}^{(+)}(\mathbf{r}). \quad (2)$$

Here the photon emission operator is defined as follows:

$$\hat{R}_{\mathbf{k}\lambda}^\dagger(\mathbf{r}) = -\sqrt{\frac{\alpha}{(2\pi)^2\omega}} \boldsymbol{\alpha} \cdot \boldsymbol{\epsilon}_\lambda^* e^{-i\mathbf{k}\cdot\mathbf{r}}, \quad (3)$$

where  $\mathbf{a}_{LM_L}^{(p)}$ 's are the magnetic ( $p = 0$ ) and electric ( $p = 1$ ) vectors,

$$\begin{aligned} \mathbf{a}_{LM_L}^{(0)}(\mathbf{r}) &= j_L(\omega r) \mathbf{Y}_{LLM_L}(\hat{\mathbf{r}}), \\ \mathbf{a}_{LM_L}^{(1)}(\mathbf{r}) &= \sqrt{\frac{L+1}{2L+1}} j_{L-1}(\omega r) \mathbf{Y}_{LL-1M_L}(\hat{\mathbf{r}}) - \sqrt{\frac{L}{2L+1}} j_{L+1}(\omega r) \mathbf{Y}_{LL+1M_L}(\hat{\mathbf{r}}), \end{aligned} \quad (8)$$

with  $j_L$  standing for the spherical Bessel function of the first kind [23] and  $\mathbf{Y}_{JLM}$  are the vector spherical harmonics [22].

where  $\boldsymbol{\alpha}$  stands for the vector of Dirac matrices and the Coulomb gauge fixes the circular polarization vector  $\boldsymbol{\epsilon}_\lambda$ . The wave functions of the incoming  $\Psi_{\mathbf{p}\mu}^{(+)}$  and outgoing  $\Psi_{\mathbf{p}\mu}^{(-)}$  electrons are given by [18–20]

$$\begin{aligned} \Psi_{\mathbf{p}\mu}^{(\pm)}(\mathbf{r}) &= \frac{1}{\sqrt{4\pi p\varepsilon}} \sum_{\kappa m_j} i^l e^{\pm i\delta_\kappa} \sqrt{2l+1} C_{l01/2\mu}^{j\mu} \\ &\times D_{m_j\mu}^j(\varphi_p, \theta_p, 0) \Psi_{\varepsilon\kappa m_j}(\mathbf{r}). \end{aligned} \quad (4)$$

Here  $\kappa = (-1)^{l+j+1/2}(j+1/2)$  is the Dirac quantum number determined by the angular momentum  $j$  and the parity  $l$ ,  $m_j$  is the angular momentum projection,  $\delta_\kappa$  is the phase shift induced by the scattering potential (for details see Appendix B),  $C_{j_1 m_1 j_2 m_2}^{JM}$  is the Clebsch-Gordan coefficient,  $D_{MM'}^J$  is the Wigner matrix [21,22], and the azimuthal  $\varphi_p$  and polar  $\theta_p$  angles define the direction of the momentum  $\mathbf{p}$ . The partial waves,

$$\Psi_{\varepsilon\kappa m_j}(\mathbf{r}) = \frac{1}{r} \begin{pmatrix} G_{\varepsilon\kappa}(r) \Omega_{\kappa m_j}(\hat{\mathbf{r}}) \\ iF_{\varepsilon\kappa}(r) \Omega_{-\kappa m_j}(\hat{\mathbf{r}}) \end{pmatrix} \quad (5)$$

are the continuum Dirac eigenstates in the scattering central potential  $V(r)$ , where  $G_{\varepsilon\kappa}$  and  $F_{\varepsilon\kappa}$  are the large and small radial components,  $\Omega_{\kappa m_j}$  is the spherical spinor [22], and  $\hat{\mathbf{r}} = \mathbf{r}/|\mathbf{r}|$ . In the present paper,  $V(r)$  is an effective (Coulomb and screening) potential created by the nucleus and target electrons,

$$V(r) = V_{\text{nuc}}(r) + V_{\text{scr}}(r) \xrightarrow{r \rightarrow +\infty} -\frac{\alpha Z_{\text{as}}}{r}, \quad (6)$$

where  $Z_{\text{as}} = Z - N_e$  with  $N_e$  being the number of target electrons. We note that the constructed wave functions of the incoming and outgoing electrons (4) effectively take into account the electron-target interaction in a nonperturbative manner.

Description of the target electrons by a spherically symmetric potential is an approximation which is well justified for the collision energies above several keV. The residual electron-correlation effects can be estimated by using different screening potentials. It was found in Ref. [3] that for neutral atoms differences between screening potentials are within 1%, and our calculations confirm this. For very low collision energies, however, the screening-potential approximation may no longer be applicable, and one can expect, e.g., the formation of resonances in the scattering process. Investigations of such effects, although extremely interesting, are beyond the scope of the present paper.

The multipole expansion of the photon field [18] is

$$\boldsymbol{\epsilon}_\lambda^* e^{-i\mathbf{k}\cdot\mathbf{r}} = \sqrt{2\pi} \sum_{LM_L} i^{-L} \sqrt{2L+1} D_{M_L\lambda}^{L*}(\varphi_k, \theta_k, 0) \sum_{p=0,1} (-i\lambda)^p \mathbf{a}_{LM_L}^{(p)*}(\mathbf{r}), \quad (7)$$

Substituting Eqs. (3) and (4) into Eq. (2) and utilizing Eqs. (5) and (7), we obtain the bremsstrahlung amplitude expressed as an infinite triple sum over the partial waves and photon multipoles,

$$\begin{aligned} \tau_{\mathbf{p}_f \mu_f, \mathbf{k} \lambda; \mathbf{p}_i \mu_i} &= \frac{1}{4\pi} \sqrt{\frac{\alpha}{2\pi\omega}} \frac{1}{\sqrt{p_i \varepsilon_i p_f \varepsilon_f}} \sum_{\kappa_i m_i} i^{l_i} e^{i\delta_{\kappa_i}} \sqrt{\frac{2l_i + 1}{2j_i + 1}} C_{l_i 0}^{j_i \mu_i} D_{m_i \mu_i}^{j_i}(\varphi_{p_i}, \theta_{p_i}, 0) \sum_{\kappa_f m_f} i^{-l_f} e^{i\delta_{\kappa_f}} \sqrt{2l_f + 1} \\ &\times C_{l_f 0}^{j_f \mu_f} D_{m_f \mu_f}^{j_f*}(\varphi_{p_f}, \theta_{p_f}, 0) \sum_{LM_L} (-i)^L \sqrt{2L + 1} C_{j_f m_f}^{j_i m_i} D_{M_L \lambda}^{L*}(\varphi_k, \theta_k, 0) \sum_{p=0,1} (-i\lambda)^p \langle \varepsilon_i \kappa_i \| \boldsymbol{\alpha} \cdot \mathbf{a}_L^{(p)*} \| \varepsilon_f \kappa_f \rangle. \end{aligned} \quad (9)$$

Here  $\langle \varepsilon_i \kappa_i \| \boldsymbol{\alpha} \cdot \mathbf{a}_L^{(p)*} \| \varepsilon_f \kappa_f \rangle$  are the reduced matrix elements whose explicit form is presented in Appendix A. Numerical evaluation of the reduced matrix elements is a difficult task. For the pure Coulomb potential, the method of calculation of these elements was worked out in Ref. [5]. Here we expand this algorithm to the case of the central potential being a superposition of the Coulomb and short-range potentials. The developed approach is discussed in details in Appendix B.

### III. NUMERICAL CALCULATIONS

Here we concentrate on the evaluation of the bremsstrahlung from electrons scattered off uranium ( $Z = 92$ ) targets in various charge states. Interest in this system is formed by a series of performed [15–17] and planned experiments. We restrict ourselves to the case when the incident electron and the target are spin unpolarized, and only the emitted photon is detected. For such a scenario, all characteristics of the process are defined by the double differential cross section (DDCS),

$$d\sigma_\lambda \equiv \frac{d\sigma_{\lambda; \mathbf{p}_i}}{d\omega d\Omega_k} = \frac{1}{2} \sum_{\mu_i \mu_f} \int d\Omega_{p_f} \frac{d\sigma_{\mathbf{p}_f \mu_f, \mathbf{k} \lambda; \mathbf{p}_i \mu_i}}{d\omega d\Omega_k d\Omega_{p_f}}. \quad (10)$$

Note that the description of the target by the effective central potential, which is used in the present paper, does not allow to take into account the polarization of the target. By calculating the transition amplitude according to Eq. (9), one obtains the DDCS as an infinite sum over the angular momentum quantum number of the incoming ( $\kappa_i$ ) and outgoing ( $\kappa_f$ ) electron and over the photon multipoles ( $L$ ). In our calculations we truncate the summation over  $\kappa_i$  and  $\kappa_f$  and perform the finite summations over all  $L$  allowed by the angular momentum selection rules. In the cases studied in the present paper, it was sufficient to truncate the summations by  $|\kappa_{i, \max}| = 2|\kappa_{f, \max}|$  and  $|\kappa_{f, \max}| = 13 \dots 17$ .

#### A. Double differential cross section

We start by studying the dependence of the DDCS on the choice of the effective screening potential. Here, we consider Perdew-Zunger (PZ) [24] and core-Hartree (CH) potentials with the latter one defined as

$$V_{\text{scr}}^{\text{(CH)}}(r) = \alpha \int_0^{+\infty} dr' \frac{\rho_e(r')}{r_>}, \quad (11)$$

where  $r_> = \max(r, r')$ , the charge density is given by

$$\rho_e(r) = \sum_{i=1}^{N_e} [G_{n_i \kappa_i}^2(r) + F_{n_i \kappa_i}^2(r)], \quad (12)$$

and normalized to the number of electrons in the target,

$$\int_0^{+\infty} dr \rho_e(r) = N_e. \quad (13)$$

Here  $G_{n_i \kappa_i}$  and  $F_{n_i \kappa_i}$  are the solutions of the Dirac equation in the combination of the nucleus field and the core-Hartree potential (11), obtained in a self-consistent manner with the use of the modified RADIAL package [25].

The normalized DDCS,

$$d\sigma = \frac{\omega}{Z^2} \sum_{\lambda=\pm 1} d\sigma_\lambda \quad (14)$$

for the bremsstrahlung from 50 and 500 keV electrons in the field of the Ne-like uranium  $\text{U}^{82+}$ , being described by different scattering potentials, is presented in Fig. 1. The energy of the emitted photon  $\omega = 0.99\varepsilon_i$ . In such a case, when the photon carries away almost the whole energy of the incoming electron, the influence of the target electrons on

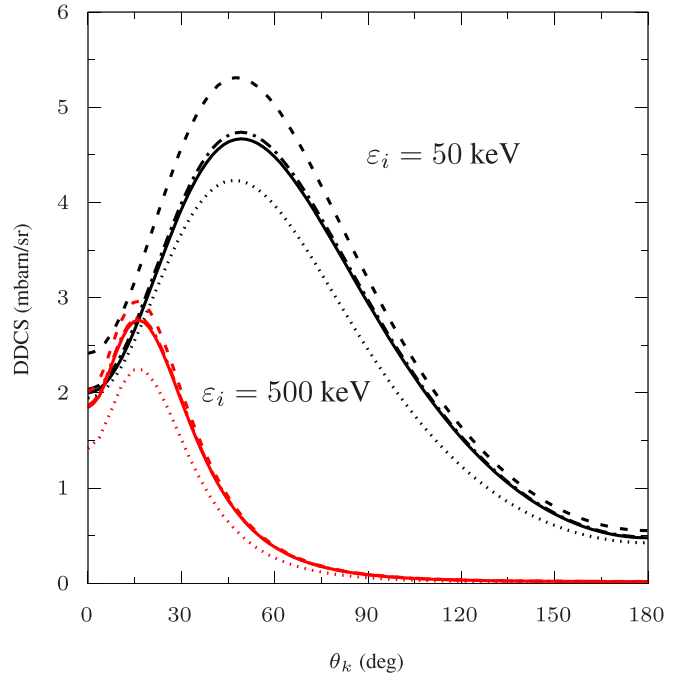


FIG. 1. Normalized double differential cross-section (14) as a function of the photon emission angle  $\theta_k$ . The incident electron with the kinetic energy  $\varepsilon_i = 50$  keV (black) and 500 keV (red) is scattered off the Ne-like uranium  $\text{U}^{82+}$ , which is described by the Coulomb potential with  $Z_{\text{as}} = 82$  (dotted), core-Hartree (solid), and Perdew-Zunger (dashed-dot) potentials. The results for the bare uranium  $\text{U}^{92+}$  (dashed) are presented as well. The photon energy  $\omega = 0.99\varepsilon_i$ .

the bremsstrahlung is the most pronounced. And, as a result, the strong dependence of the DDCCS on the choice of the screening potential is expected. From Fig. 1, it is seen that the difference between the DDCCS, calculated with the CH and PZ scattering potentials, is negligible. In what follows, therefore, we perform the calculations only with the core-Hartree potential. Although the form of the screening potential almost does not affect the results, taking into account of the short-range potential leads to prominent changes in the DDCCS, which correspond to a rather large difference between the dotted and solid lines in the figure. This difference amounts to about 10% and 20% for low and high kinetic energies of the incident electron. Figure 1 also shows that the cross sections for the screening potentials lie in between the values for the purely Coulomb potentials with the charges  $Z$  and  $Z_{as}$ . This can be explained as follows. In the case of the screening potential, the incoming electron can penetrate the repulsion field of the target electrons and decelerate via photon emission in the vicinity of the nucleus. In this region, the nucleus charge is almost unscreened, thus, resulting in the shift of the cross section for the pure Coulomb potential with the charge  $Z_{as}$  toward the one for  $Z$ .

We now turn to the investigation of dependence of the bremsstrahlung DDCCS (14) on the number of target electrons  $N_e$ . In Figures 2–4, we present the results for the bremsstrahlung of 50–, 100–, and 500-keV electrons, respectively, in the fields of the bare, Ne-like, Xe-like, and neutral uranium targets. The scattering potential of the neutral atom is described by a sum of three Yukawa terms [26,27],

$$V_{\text{neut}}(r) = -\frac{\alpha Z}{r} \sum_{i=1}^3 A_i e^{-\alpha_i r}, \quad (15)$$

with  $A_i$  and  $\alpha_i$  standing for the potential amplitude and scaling constant, respectively. We note that our results for the neutral atom are in good agreement with ones from Ref. [5] where completely different algorithms have been utilized. From Fig. 2, it is seen that for low energies of the incident electron, the dependence on the number of target electrons becomes the most prominent. In contrast, at high energies, the differences in the DDCCS for different charge states of the target become smaller. This can be explained as follows. The bremsstrahlung from high-energy electrons comes mainly from the region close to the nucleus, whereas the contribution from the target electrons is of minor importance. For incident electrons with low energies, the region of the dominant contribution is shifted to distances that are closer to the spectator electrons and, as a result, the dependence on the number of the target electrons increases. It should also be mentioned that the emitted photons with the energies  $\omega = 0.99\varepsilon_i$  are mostly emitted in the course of bremsstrahlung from the nuclear region. In this case, as can be seen from Figs. 2–4, the curves corresponding to the different charge states of the target lay closer to each other when compared to other photon energies.

### B. Stokes parameters

To study the polarization properties of the bremsstrahlung, we consider the Stokes parameters defined

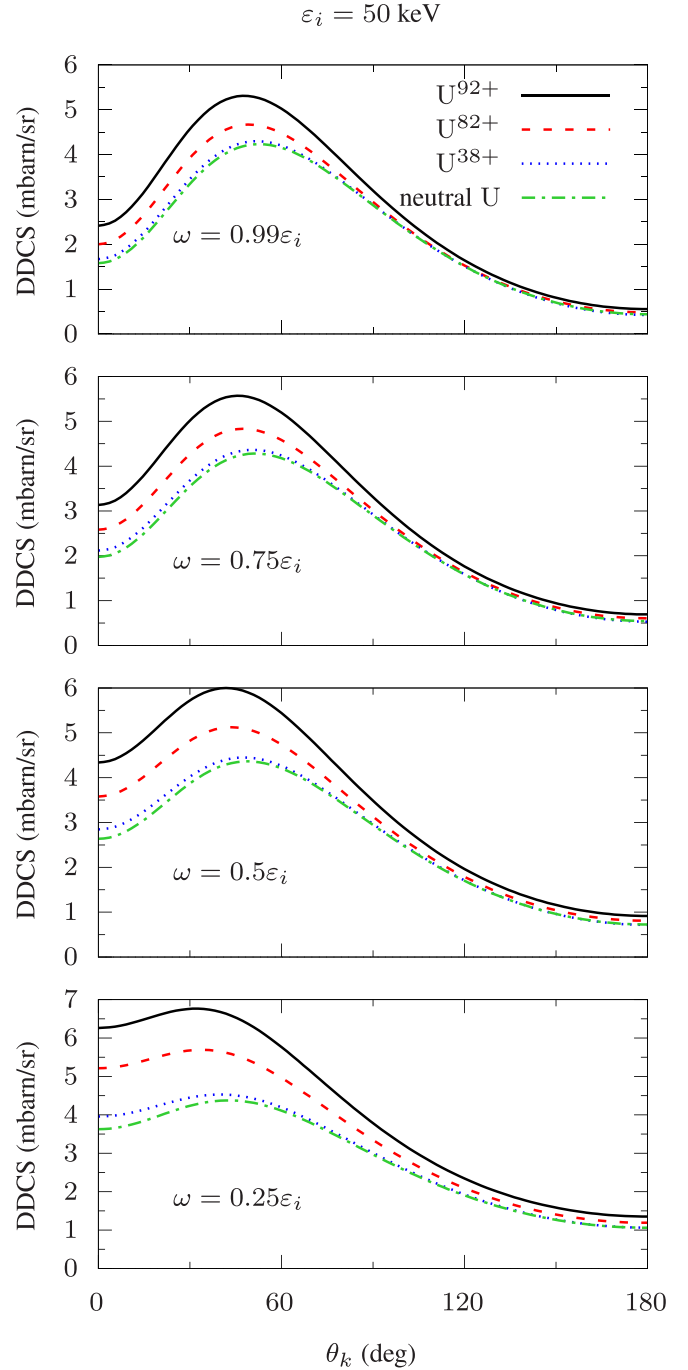
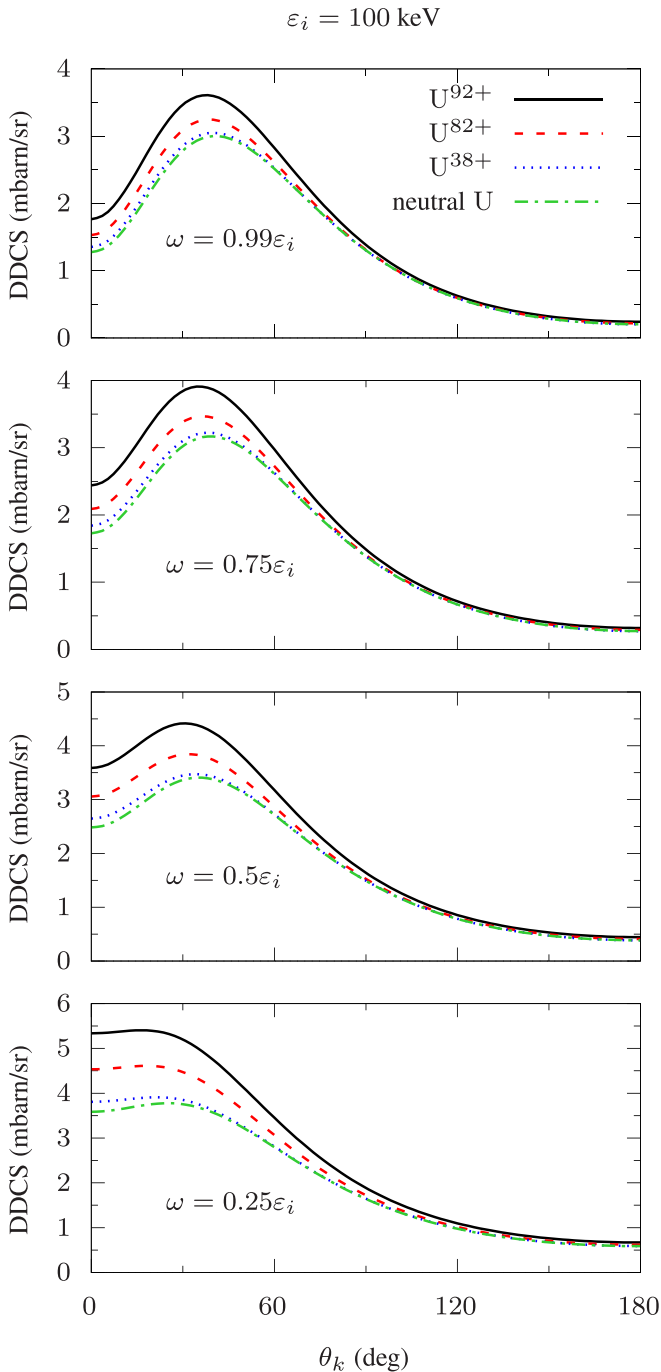


FIG. 2. Normalized double differential cross-section (14) as a function of the photon emission angle  $\theta_k$ . The results are represented for the bare  $U^{92+}$  (black solid), Ne-like  $U^{82+}$  (red dashed), Xe-like  $U^{38+}$  (blue dotted), and neutral (green dashed-dot) uranium targets. The incident electron kinetic energy is  $\varepsilon_i = 50$  keV. The photon energies  $\omega$  are as shown in the panels.

by

$$P_1 = \frac{d\sigma_{0^\circ} - d\sigma_{90^\circ}}{d\sigma_{0^\circ} + d\sigma_{90^\circ}}, \quad P_2 = \frac{d\sigma_{45^\circ} - d\sigma_{135^\circ}}{d\sigma_{45^\circ} + d\sigma_{135^\circ}},$$

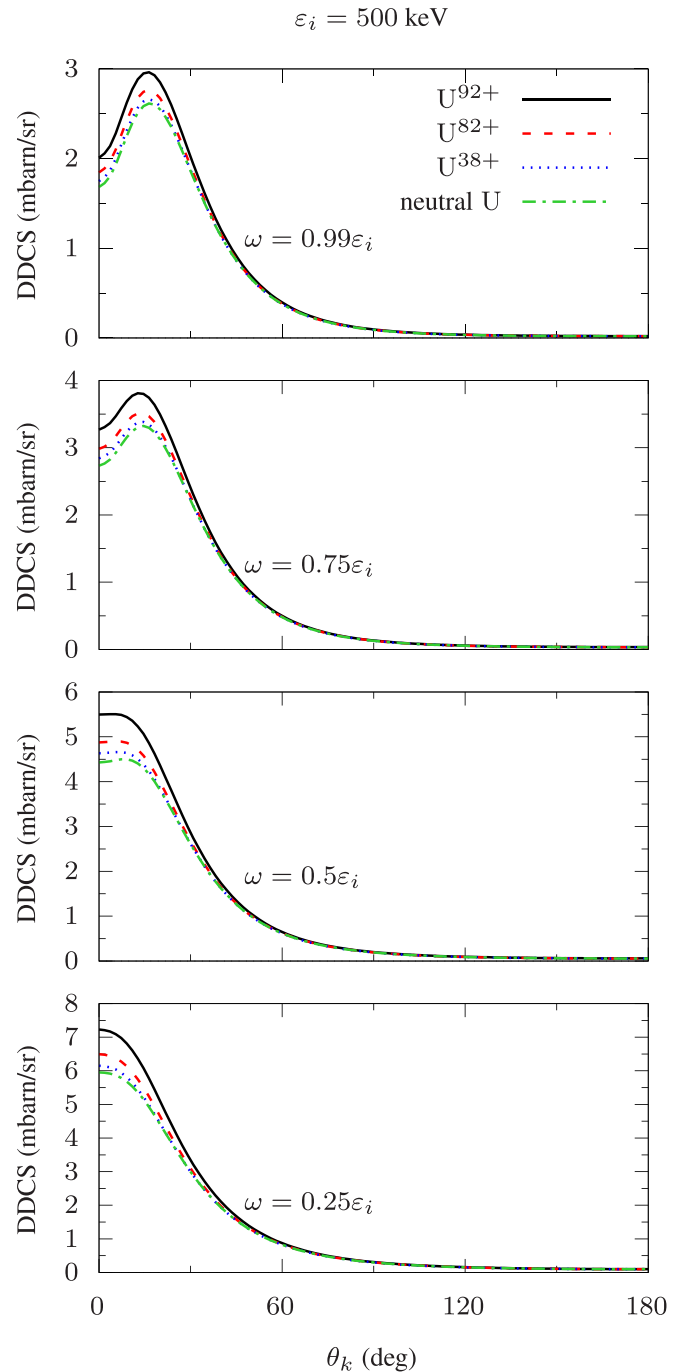
$$P_3 = \frac{d\sigma_{+1} - d\sigma_{-1}}{d\sigma_{+1} + d\sigma_{-1}}. \quad (16)$$


 FIG. 3. The same as Fig. 2 but for  $\epsilon_i = 100$  keV.

Here  $d\sigma_\chi$  stands for the DDCS (10) of the linear polarized bremsstrahlung with the polarization angle  $\chi$ , whereas  $d\sigma_{+1}$  and  $d\sigma_{-1}$  are the cross sections for the emission of right and left circularly polarized photons, respectively. To obtain the expression for  $d\sigma_\chi$ , one needs to replace  $\epsilon_\lambda$  in Eq. (3) with the vector of the linear polarization,

$$\epsilon_\chi = \frac{1}{\sqrt{2}} \sum_{\lambda=\pm 1} e^{i\lambda\chi} \epsilon_\lambda. \quad (17)$$

Since the incident electron and the target are spin unpolarized,  $P_2$  and  $P_3$  are identically equal to zero [4]. Therefore, only the degree of linear polarization  $P_1$  is relevant. In Fig. 5, the


 FIG. 4. The same as Fig. 2 but for  $\epsilon_i = 500$  keV.

Stokes parameter  $P_1$  is shown as a function of the photon emission angle  $\theta_k$  for the same set of the parameters as in Figs. 2–4. From this figure, it is seen that the dependence of  $P_1$  on the number of target electrons is barely recognizable.

### C. Radiative electron capture to the continuum

In collisions of highly charged heavy ions with light atoms or molecules, an ion can capture an electron from the target discrete spectrum. If the electron is captured to the projectile continuum and one photon is emitted, the process is called RECC. A theoretical description of RECC was first presented by Jakubassa-Amundsen in a series of papers [28–31].

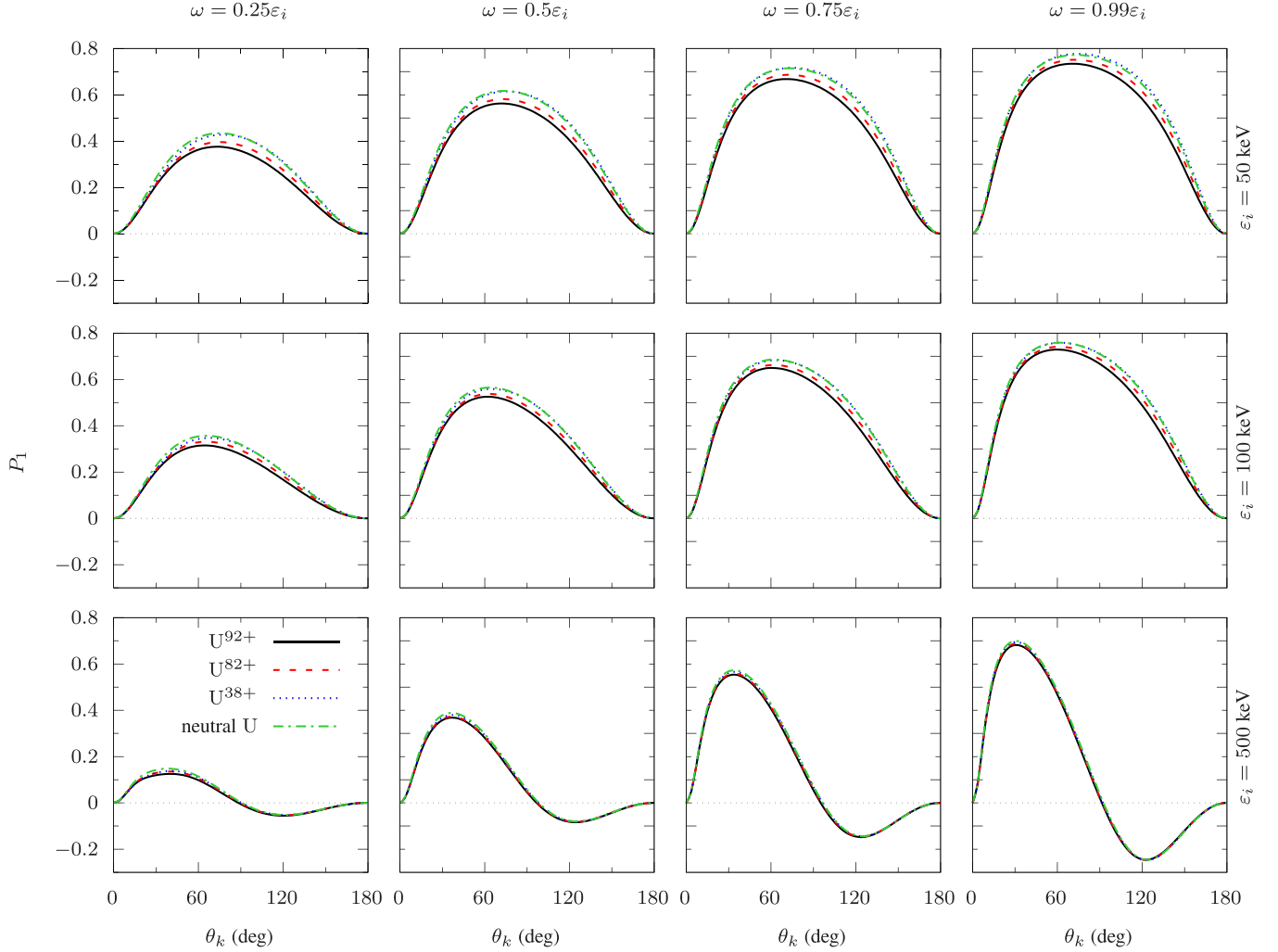
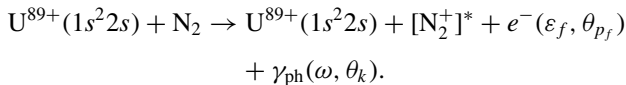


FIG. 5. The degree of linear polarization  $P_1$  as a function of the photon emission angle  $\theta_k$ . The results are represented for the bare  $U^{92+}$  (black solid), Ne-like  $U^{82+}$  (red dashed), Xe-like  $U^{38+}$  (blue dotted), and neutral (green dashed-dot) uranium targets. The first, second, and third rows correspond to the incident electron kinetic energies  $\varepsilon_i = 50, 100,$  and  $500$  keV, respectively. The photon energies  $\omega = 0.25\varepsilon_i, 0.5\varepsilon_i, 0.75\varepsilon_i,$  and  $0.99\varepsilon_i$  are presented in the first, second, third, and fourth columns, respectively.

Measurements of the RECC allow one to study electron bremsstrahlung at the high-energy endpoint. At this endpoint where the emitted photon carries away the highest possible energy, the bremsstrahlung emission exhibits the most strong dependence on the charge state of the projectile.

With this in mind, we turn to the theoretical description of the RECC channel in the collision of Li-like uranium ions with a supersonic gas-jet target of molecular nitrogen,



This process was experimentally studied just recently in Ref. [17]. In the projectile reference frame, the RECC process is related to the high-energy endpoint of the bremsstrahlung from the target quasifree electrons scattered off the heavy projectile. Utilizing this relation and approximating the field of the Li-like uranium by the pure Coulomb potential with the charge  $Z = 89$ , the theoretical description has been performed. Such a description accounts for the presence of the target electrons only by means of the effective nuclear charge.

However, for considered energies of the incident quasifree electrons  $\varepsilon'_i = 41.64$  keV (here and throughout, primes refer to the variables defined in the projectile reference frame), the electronic structure can provide a significant contribution to the cross section. Here we evaluate this contribution with the usage of the developed algorithm.

To compare the theoretical results with the measured  $0^\circ$  electron spectra of the RECC one needs to average the bremsstrahlung triple differential cross section (TDCS) over laboratory-frame polar  $\theta_{p_f}$  and azimuthal  $\varphi_{p_f}$  angles as follows [16,17]:

$$\begin{aligned} \left. \frac{d\sigma_{\mathbf{p}_i}^{(RECC)}}{d\omega d\Omega_k d\Omega_{p_f}} \right|_{\theta_{p_f}=0^\circ} &= \frac{Z_t}{\gamma^2(1 - \beta \cos \theta_k)^2} \\ &\times \int_0^{\theta_{\max}} d\theta_{p_f} \frac{\sin \theta'_{p_f}}{1 - \cos \theta_{\max}} \\ &\times \int_0^{2\pi} \frac{d\varphi_{p_f}}{2\pi} \sum_{\lambda} \frac{d\sigma_{\lambda; \mathbf{p}_i}^{(brem)}}{d\omega' d\Omega'_k d\Omega'_{p_f}}. \end{aligned} \tag{18}$$

Here  $Z_t = 7$  is the nuclear charge of the target nitrogen atom,  $\beta = 0.3808$  and  $\gamma = 1.081$  are the velocity and Lorentz factors of the projectile, respectively, and the prefactor originates from the relation between the solid angles in the projectile  $d\Omega'_k$  and laboratory  $d\Omega_k$  frames (see, e.g., Ref. [32]),

$$\frac{d\Omega'_k}{d\Omega_k} = \frac{1}{\gamma^2(1 - \beta \cos \theta_k)^2}. \quad (19)$$

The bremsstrahlung TDCS is averaged over the initial and summed over final polarizations and averaging over  $0^\circ \leq \theta_{p_f} \leq \theta_{\max}$  and  $0^\circ \leq \varphi_{p_f} < 360^\circ$  covered by the spectrometer is held. The emission angles of the scattered electron  $\theta'_{p_f}$  and emitted photon  $\theta'_k$  in the projectile frame are connected to the observation angles  $\theta_{p_f}$  and  $\theta_k$  in the target frame as follows:

$$\theta'_{p_f} = \pi - \arctan \left[ \frac{\sin \theta_{p_f}}{\gamma(\cos \theta_{p_f} - \beta \varepsilon_f / p_f)} \right], \quad (20)$$

$$\theta'_k = \pi - \arctan \left[ \frac{\sin \theta_k}{\gamma(\cos \theta_k - \beta)} \right]. \quad (21)$$

The relation of the projectile-frame energies  $\varepsilon'_f$  and  $\omega'$  to the corresponding observables in the target frame is given by the Lorentz transformation,

$$\varepsilon'_f = \varepsilon_f + \gamma \varepsilon_f - \gamma \beta p_f \cos \theta_{p_f}, \quad (22)$$

$$\omega' = \gamma \omega (1 - \beta \cos \theta_k). \quad (23)$$

We fix the photon emission angle  $\theta_k = 90^\circ$  ( $\theta'_k = 67.6^\circ$  in the projectile reference frame) and the maximal polar angle  $\theta_{\max} = 3.0^\circ$  to match the conditions in Ref. [17].

In Fig. 6, the TDCS of RECC is presented as a function of the captured electron energy in the laboratory (target) frame. The experimental TDCS measured on a relative scale were normalized to the theoretical results employing the core-Hartree potential. Note that the experimental data points for the energies below the cusp energy (in the target frame) sometimes have negative values. It is a consequence of the applied background correction, in which the background counts are subtracted from the total number of counts. From Fig. 6, it is seen that the results obtained for the core-Hartree potential, which effectively accounts for the interaction of the quasifree electron with the Li-like uranium ion, differs from the ones obtained for the pure Coulomb potential. We conclude that taking into account the screening effects leads to significant changes in TDCS. As the photon energy  $\omega'$  approaches the initial kinetic energy of the electron  $\varepsilon'_i$ , the difference between two theoretical curves increases and reaches 14% at the high-energy endpoint. At lower photon energies, the deviation is about 10%. The uncertainty of the experimental data from Ref. [17] was dominated by the statistical uncertainty, which could be reduced straightforward in a future measurement. Therefore, such a deviation can, in principle, be detected in experiment. This justifies the importance of the calculations accounting for the electron-target interaction in a nonperturbative regime.

#### IV. CONCLUSION

In this paper, we have presented the fully relativistic description of the electron bremsstrahlung in the field of ionic

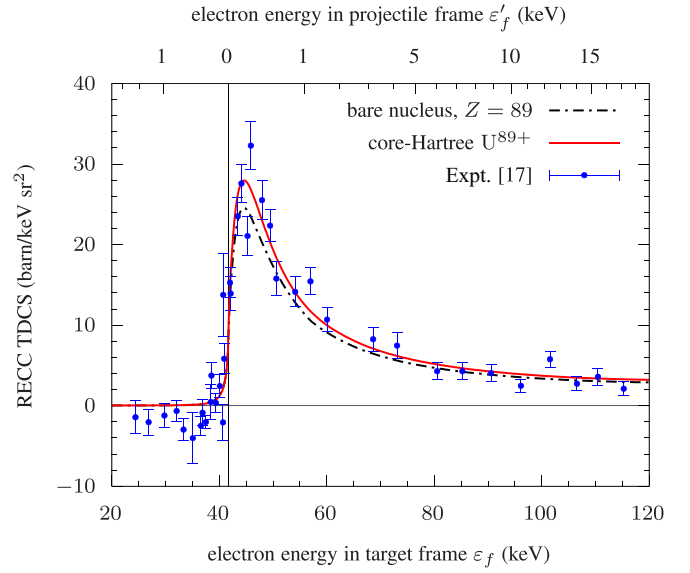


FIG. 6. The RECC triple differential cross section as a function of the measured electron energy. The photon emission angle is fixed as  $\theta_k = 90^\circ$  and the TDCS is averaged over  $0^\circ \leq \theta_{p_f} \leq 3.0^\circ$  and  $0^\circ \leq \varphi_{p_f} < 360^\circ$ . The results are shown for  $U^{89+}$  described by the core-Hartree potential (red solid) and pure Coulomb potential with  $Z = 89$  (black dashed dot). Experimental data from Ref. [17] are represented by (blue) solid circles with error bars due to the statistical uncertainty.

targets. The electron-target interaction was treated nonperturbatively by using solutions of the Dirac equation for the combination of the Coulomb and the screening potentials for the incoming and outgoing electrons. In the case of the pure Coulomb and a finite-range potential, our calculations were shown to agree with those reported in Ref. [5].

The developed approach was applied to the evaluation of the double differential cross sections and Stokes parameters of the bremsstrahlung from the bare, Ne-like, Xe-like, and neutral uranium. We found that for 50-keV incident electrons taking into account the screening effects alters the double differential cross section by 10–20% as compared to the case of the pure Coulomb potential. In contrast, the linear polarization of the bremsstrahlung was shown to be insensitive to the charge state of the target.

Furthermore, we have applied the developed method to the calculation of the radiative electron capture to the continuum in the collision of the Li-like uranium ions with molecular nitrogen, which was experimentally studied recently in Ref. [17]. It was demonstrated that accounting for the electronic structure of  $U^{89+}$  projectile results in significant changes in the triple differential cross section. The changes as high as 14% were found in comparison with the results obtained for the pure Coulomb potential with the effective charge  $Z = 89$  (used in Ref. [17]). Effects of this magnitude can be detected in modern experiments at heavy-ion storage rings. We conclude that the screening effects should be taken into account in the theoretical description of the electron bremsstrahlung from the highly charged ions in the energy region of a few tens of keV.

On the experiment side, heavy-ion storage rings offer flexible conditions regarding the collision systems where intense beams of basically any element in a selected charge state can be provided for collisions with any gaseous internal target [33]. With the commissioning of FAIR, such highly charged ion beams will be available in a broad range of energies from basically at rest up to a few GeV/u [34]. The developed here methodology is important for guiding current as well as future experiments.

### ACKNOWLEDGMENTS

The work was supported by the German-Russian Interdisciplinary Science Center (G-RISC Sur-Place Stipend No. F-2021b-25). V.M.S. acknowledges support from RFBR and ROSATOM according to the Research Project No. 20-21-00098. The work of M.E.G., V.A.Z., and V.A.Y. was supported by the Russian Science Foundation (Grant No. 20-62-46006).

### APPENDIX A: REDUCED MATRIX ELEMENTS

Results for the reduced matrix elements in Eq. (9) are

$$\begin{aligned} (-i)\langle \varepsilon_i \kappa_i \| \boldsymbol{\alpha} \cdot \mathbf{a}_L^{(0)*} \| \varepsilon_f \kappa_f \rangle &= P_{LL}(i, f), \\ (-i)\langle \varepsilon_i \kappa_i \| \boldsymbol{\alpha} \cdot \mathbf{a}_L^{(1)*} \| \varepsilon_f \kappa_f \rangle &= \sqrt{\frac{L+1}{2L+1}} P_{LL-1}(i, f) \\ &\quad - \sqrt{\frac{L}{2L+1}} P_{LL+1}(i, f). \end{aligned} \quad (\text{A1})$$

$$\begin{pmatrix} G_{\varepsilon\kappa}^{(\text{reg})} \\ F_{\varepsilon\kappa}^{(\text{reg})} \end{pmatrix} = N \begin{pmatrix} p\sqrt{\gamma^2 + v^2}(\gamma + \kappa)F_\gamma(-v, pr) + \alpha Z_{\text{as}}(\varepsilon\kappa - \gamma m_e)F_{\gamma-1}(-v, pr) \\ \alpha Z_{\text{as}}p\sqrt{\gamma^2 + v^2}F_\gamma(-v, pr) + (\gamma + \kappa)(\varepsilon\kappa - \gamma m_e)F_{\gamma-1}(-v, pr) \end{pmatrix}, \quad (\text{B2})$$

$$\begin{pmatrix} G_{\varepsilon\kappa}^{(\text{irr})} \\ F_{\varepsilon\kappa}^{(\text{irr})} \end{pmatrix} = N \begin{pmatrix} p\sqrt{\gamma^2 + v^2}(\gamma + \kappa)G_\gamma(-v, pr) + \alpha Z_{\text{as}}(\varepsilon\kappa - \gamma m_e)G_{\gamma-1}(-v, pr) \\ \alpha Z_{\text{as}}p\sqrt{\gamma^2 + v^2}G_\gamma(-v, pr) + (\gamma + \kappa)(\varepsilon\kappa - \gamma m_e)G_{\gamma-1}(-v, pr) \end{pmatrix}. \quad (\text{B3})$$

Here  $N$  is the normalization factor defined as

$$N = \sqrt{\frac{\varepsilon + m_e}{\pi p}} \frac{1}{\gamma \sqrt{p^2(\gamma + \kappa)^2 + \alpha^2 Z_{\text{as}}^2(\varepsilon + m_e)^2}}, \quad (\text{B4})$$

with  $\gamma = \sqrt{\kappa^2 - (\alpha Z_{\text{as}})^2}$  and the Sommerfeld parameter  $\nu = \alpha Z_{\text{as}}\varepsilon/p$ . The Coulomb functions in (B2) and (B3) can be expressed through the Whittaker functions of the second kind  $W_{\alpha, \beta}$  as follows [23]:

$$F_\lambda(\eta, \rho) = \frac{H_\lambda^+(\eta, \rho) - H_\lambda^-(\eta, \rho)}{2i}, \quad G_\lambda(\eta, \rho) = \frac{H_\lambda^+(\eta, \rho) + H_\lambda^-(\eta, \rho)}{2}, \quad (\text{B5})$$

$$H_\lambda^\pm(\eta, \rho) = e^{\pi\eta/2} \exp\left\{\mp i\left[\frac{\pi\lambda}{2} - \sigma_\lambda(\eta)\right]\right\} W_{\mp i\eta, \lambda+1/2}(\mp 2i\rho), \quad (\text{B6})$$

with  $\sigma_\lambda(\eta)$  standing for the argument of the Euler's gamma function  $\Gamma(\lambda + 1 + i\eta)$  [23].

Since the integrand in (A2) is an oscillating function, we apply the rotation of the integration path into the complex plane. For this purpose, the integral  $P_{JL}(i, f)$  is divided into two parts,

$$P_{JL}(i, f) = P_{JL}^{(R)}(i, f) + P_{JL}^{(C)}(i, f), \quad (\text{B7})$$

Here the radial integrals are given by

$$\begin{aligned} P_{JL}(i, f) &= \int_0^{+\infty} dr j_L(\omega r) [S_{JL}(\kappa_i, -\kappa_f) G_{\varepsilon_i \kappa_i}(r) F_{\varepsilon_f \kappa_f}(r) \\ &\quad - S_{JL}(-\kappa_i, \kappa_f) G_{\varepsilon_f \kappa_f}(r) F_{\varepsilon_i \kappa_i}(r)], \end{aligned} \quad (\text{A2})$$

where the angular coefficients  $S_{JL}(\kappa_i, \kappa_f)$  are defined as in Ref. [5],

$$S_{JL}(\kappa_i, \kappa_f) = (-1)^{l_f} \sqrt{\frac{3}{2\pi}} \Pi_{j_i j_f l_i l_f} C_{l_i 0 l_f 0}^{L 0} \begin{Bmatrix} j_i & l_i & 1/2 \\ j_f & l_f & 1/2 \\ J & L & 1 \end{Bmatrix}, \quad (\text{A3})$$

with  $\Pi_{ab\dots c} = \sqrt{(2a+1)(2b+1)\dots(2c+1)}$  and  $\{\dots\}$  stands for  $9j$  symbol [22].

### APPENDIX B: RADIAL FUNCTIONS

Outside the finite-range potential, the radial parts of the electron continuum wave functions are expressed through the solutions of the Dirac equation in the pure Coulomb potential with the effective asymptotic charge  $Z_{\text{as}}$  as follows:

$$(G_{\varepsilon\kappa} \ F_{\varepsilon\kappa}) = \cos \delta_{\text{scr}} (G_{\varepsilon\kappa}^{(\text{reg})} \ F_{\varepsilon\kappa}^{(\text{reg})}) + \sin \delta_{\text{scr}} (G_{\varepsilon\kappa}^{(\text{irr})} \ F_{\varepsilon\kappa}^{(\text{irr})}), \quad (\text{B1})$$

where the phase shift  $\delta_{\text{scr}}$  is induced by the short-range screening potential. This phase shift is calculated with the use of the modified RADIAL package [25] by matching the inner solutions for the finite-range potential with the asymptotic point-Coulomb Dirac solutions as described in Ref. [25]. The regular and irregular at origin solutions can be expressed in terms of the Coulomb functions [23,25],

where the first part,

$$P_{JL}^{(R)}(i, f) = \int_0^R dr j_L(\omega r) [S_{JL}(\kappa_i, -\kappa_f) G_{\varepsilon_i \kappa_i}(r) F_{\varepsilon_f \kappa_f}(r) - S_{JL}(-\kappa_i, \kappa_f) G_{\varepsilon_f \kappa_f}(r) F_{\varepsilon_i \kappa_i}(r)] \quad (\text{B8})$$

is calculated numerically utilizing functions and subroutines from the modified RADIAL package [25]. The remaining part,

$$P_{JL}^{(C)}(i, f) = \int_R^{+\infty} dr j_L(\omega r) [S_{JL}(\kappa_i, -\kappa_f) G_{\varepsilon_i \kappa_i}(r) F_{\varepsilon_f \kappa_f}(r) - S_{JL}(-\kappa_i, \kappa_f) G_{\varepsilon_f \kappa_f}(r) F_{\varepsilon_i \kappa_i}(r)] \quad (\text{B9})$$

is a linear combination of integrals,

$$I \equiv I_{\alpha_i, \beta_i; \alpha_f, \beta_f; L}(s_i, s_f) = \int_R^{+\infty} dr j_L(\omega r) W_{\alpha_i, \beta_i}(2ip_i s_i r) W_{\alpha_f, \beta_f}(2ip_f s_f r), \quad (\text{B10})$$

where  $s_i$  and  $s_f$  are equal to  $+1$  or  $-1$ . The point  $R$  is chosen so that for  $r > R$  the asymptotics of all appearing Whittaker functions,

$$W_{\alpha, \beta}(z) \xrightarrow{|z| \rightarrow +\infty} e^{-z/2} z^\alpha \left[ \sum_{n=0}^{N-1} \frac{(1/2 - \alpha + \beta)_n (1/2 - \alpha - \beta)_n}{n!} (-z)^{-n} + O(|z|^{-N}) \right] \quad (\text{B11})$$

converge with the required accuracy. Here  $(x)_n = x(x+1)\cdots(x+n-1)$  stands for the Pochhammer's symbol [23]. It can be seen from (B11) that the Whittaker functions  $W_{\alpha, \beta}(2ipr)$  and  $W_{\alpha, \beta}(-2ipr)$  are regular in the lower and upper halves of the complex  $r$  plane, respectively. They both decrease exponentially with  $r$  moving away from the real axis. Substituting (B11) into (B10) and utilizing the explicit form of Bessel functions [23],

$$j_L(z) = \sum_{s=\pm 1} \sum_{n=0}^L (-is)^{L+1-n} \frac{(L+n)!}{n!(L-n)!} \frac{e^{isz}}{(2z)^{n+1}}, \quad (\text{B12})$$

we arrive at

$$I = \int_R^{+\infty} dr r^{\alpha_i + \alpha_f - 1} \sum_{s=\pm 1} e^{i(s\omega - s_i p_i - s_f p_f)r} \sum_{n \geq 0} \frac{c_n}{r^n}. \quad (\text{B13})$$

Since for the bremsstrahlung process  $p_i > p_f + \omega$ , we perform the  $\pi/2$  rotation of the integration path to the upper half of the complex  $r$  plane for  $s_i = -1$  and to the lower one for  $s_i = +1$ . Employing the change in variables  $r = R + is_i \xi$  gives us the converging factor  $e^{-p_i \xi}$  in each integral  $I$ .

- 
- [1] A. Mangiarotti and M. N. Martins, *Radiat. Phys. Chem.* **141**, 312 (2017).
- [2] D. H. Jakubassa-Amundsen, [arXiv:2103.06034](https://arxiv.org/abs/2103.06034).
- [3] H. K. Tseng and R. H. Pratt, *Phys. Rev. A* **3**, 100 (1971).
- [4] H. K. Tseng and R. H. Pratt, *Phys. Rev. A* **7**, 1502 (1973).
- [5] V. A. Yerokhin and A. Surzhykov, *Phys. Rev. A* **82**, 062702 (2010).
- [6] S. Tashenov, T. Bäck, R. Barday, B. Cederwall, J. Enders, A. Khaplanov, Y. Fritzsche, K.U. Schüssburger, A. Surzhykov, V. A. Yerokhin, and D. Jakubassa-Amundsen, *Phys. Rev. A* **87**, 022707 (2013).
- [7] R. A. Müller, V. A. Yerokhin, and A. Surzhykov, *Phys. Rev. A* **90**, 032707 (2014).
- [8] A. Pořkus, *Comput. Phys. Commun.* **232**, 237 (2018).
- [9] A. Pořkus, *At. Data Nucl. Data Tables* **129**, 101277 (2019).
- [10] D. H. Jakubassa-Amundsen and A. Mangiarotti, *Phys. Rev. A* **100**, 032703 (2019).
- [11] D. H. Jakubassa-Amundsen, *Phys. Rev. A* **82**, 042714 (2010).
- [12] D. H. Jakubassa-Amundsen, *Phys. Rev. A* **98**, 062715 (2018).
- [13] D. H. Jakubassa-Amundsen, *J. Phys. G: Nucl. Part. Phys.* **47**, 075102 (2020).
- [14] D. H. Jakubassa-Amundsen, *Phys. Rev. A* **93**, 052716 (2016).
- [15] M. Nofal, S. Hagmann, T. Stöhlker, D. H. Jakubassa-Amundsen, C. Kozhuharov, X. Wang, A. Gumberidze, U. Spillmann, R. Reuschl, S. Hess, S. Trotsenko, D. Banas, F. Bosch, D. Liesen, R. Moshhammer, J. Ullrich, R. Dörner, M. Steck, F. Nolden, P. Beller, H. Rothard, K. Beckert, and B. Franczak, *Phys. Rev. Lett* **99**, 163201 (2007).
- [16] P.-M. Hillenbrand, S. Hagmann, D. Atanasov, D. Banaś, K.-H. Blumenhagen, C. Brandau, W. Chen, E. De Filippo, A. Gumberidze, D. L. Guo, D. H. Jakubassa-Amundsen, O. Kovtun, C. Kozhuharov, M. Lestinsky, Y. A. Litvinov, A. Müller, R. A. Müller, H. Rothard, S. Schippers, M. S. Schöffler, U. Spillmann, A. Surzhykov, S. Trotsenko, N. Winckler, X. L. Yan, V. A. Yerokhin, X. L. Zhu, and T. Stöhlker, *Phys. Rev. A* **90**, 022707 (2014).
- [17] P.-M. Hillenbrand, S. Hagmann, M. E. Groshev, D. Banaś, E. P. Benis, C. Brandau, E. De Filippo, O. Forstner, J. Glorius, R. E. Grisenti, A. Gumberidze, D. L. Guo, B. Hai, M. O. Herdrich, M. Lestinsky, Y. A. Litvinov, E. V. Pagano, N. Petridis, M. S. Sanjari, D. Schury, U. Spillmann, S. Trotsenko, M. Vockert, G. Weber, V. A. Yerokhin, and T. Stöhlker, *Phys. Rev. A* **101**, 022708 (2020).
- [18] M. E. Rose, *Relativistic Electron Theory* (Wiley, New York, 1961).
- [19] R. H. Pratt, A. Ron, and H. K. Tseng, *Rev. Mod. Phys.* **45**, 273 (1973); **45**, 663(E) (1973).
- [20] J. Eichler and W. Meyerhof, *Relativistic Atomic Collisions* (Academic, San Diego, 1995).
- [21] M. E. Rose, *Elementary Theory of Angular Momentum*, (Wiley, New York, 1957).

- [22] D. A. Varshalovich, A. N. Moskalev, and V. K. Khersonskii, *Quantum Theory of Angular Momentum* (World Scientific, Singapore, 1988).
- [23] *Handbook of Mathematical Functions*, edited by M. Abramovitz and I. A. Stegun (U.S. Govt. Printing Office, Washington, DC, 1964).
- [24] J. P. Perdew and A. Zunger, *Phys. Rev. B* **23**, 5048 (1981).
- [25] F. Salvat, J. M. Fernández-Varea, and W. Williamson, Jr., *Comput. Phys. Commun.* **90**, 151 (1995).
- [26] F. Salvat, J. D. Martinez, R. Mayol, and J. Parellada, *Phys. Rev. A* **36**, 467 (1987).
- [27] F. Salvat, *Phys. Rev. A* **43**, 578 (1991).
- [28] D. H. Jakubassa-Amundsen, *J. Phys. B: At., Mol. Opt. Phys.* **36**, 1971 (2003).
- [29] D. H. Jakubassa-Amundsen, *Radiat. Phys. Chem.* **75**, 1319 (2006).
- [30] D. H. Jakubassa-Amundsen, *J. Phys. B: At., Mol. Opt. Phys.* **40**, 2719 (2007).
- [31] D. H. Jakubassa-Amundsen, *Eur. Phys. J. D* **41**, 267 (2007).
- [32] J. Eichler and T. Stöhlker, *Phys. Rep.* **439**, 1 (2007).
- [33] M. Steck and Y. Litvinov, *Prog. Part. Nucl. Phys.* **115**, 103811 (2020).
- [34] T. Stöhlker *et al.*, *Nucl. Instrum. Methods Phys. Res., Sect. B* **365**, 680 (2015).